Thermal properties of $60P_2O_5$–$(40-x)Al_2O_3$–xNa_2O glasses

Małgorzata Ciecińska[1] · Paweł Goj[1] · Agata Stoch[2] · Paweł Stoch[1]

Abstract

Phosphate glasses are important materials in many fields. However, their usage can be limited due to water corrosion. Addition of Al_2O_3 significantly improves the water resistance, and as such, the glass of superior water durability can be obtained. Thus, it may be considered as a matrix for waste immobilization. In the paper, thermal properties of $60P_2O_5$–$(40-x)Al_2O_3$–xNa_2O glasses are presented. The materials were investigated with the application of DSC/TG method and observations of shape change during heating in a heating microscope. Water durability studies are also presented. It was evidenced that glass of low Na_2O content crystallizes during heating, which limits their application in waste vitrification. Nevertheless, the obtained glass–ceramic material is characterized by a superior water resistance. The water durability decreases with sodium content. The obtained results are discussed from a waste immobilization point of view, and the optimal glass composition containing 15 mol% of Na_2O is indicated due to it low viscosity, melting temperature and very good water resistance.

Keywords Phosphate glasses · Heating microscopy · DSC/TG analysis · Leachability

Introduction

Phosphate glasses are important materials which offer great application potential. Their high thermal expansion coefficient and low liquidus temperature make them suitable as sealants with metals and alloys [1]. The glasses containing Ca can be biocompatible and can be used as bone or dental implants [2–7]. Addition of rare earths makes them attractive materials for laser and optoelectronic devices [8–14]. Phosphate glasses can be also used as fertilizers of slow and controlled dissolution [15–17]. One of the biggest drawbacks of the phosphate glasses can be the abundance of easily hydrated P–O–P bonds, which strongly limit their practical applications [18, 19]. However, the addition of iron or aluminum oxides replaces P–O–P bonds by more chemically durable P–O–Fe/Al and significantly increases the chemical durability of the glasses, and as a consequence, a superior water-resistant material can be obtained [20, 21]. Thus, the glasses can be very attractive for the vitrification process of toxic or radioactive waste. The glasses are now considered as a matrix for vitrification of waste which by its composition cannot be immobilized in "conventional" borosilicate glasses. Such waste can contain a high concentration of actinides, salts such as cesium sulfate, and chlorides [22–25]. Additionally, the glasses are characterized by lower melting temperatures and viscosity of the melt comparing to borosilicate, which leads to a decrease in the vitrification temperature and homogenization time. Thus, evaporation of volatile components, the creation of secondary waste from off-gas systems and costs of the process are limited [25, 26].

Pure or P_2O_5-rich glasses are unstable in the air due to their corrosion by water from a humid environment. Water can hydrolyze covalent P–O–P bonds or hydrate modifier cations. Generally, P–O–P chains are disrupted and hydroxyls groups P–OH are formed. The breaking of chains lowers the glass network polymerization, and the network swells to form a gelatinous layer [27]. Additionally, water can form modifier hydrates such as NaOH, which increase the glass corrosion level [28, 29]. Water adsorption by the glass network increases with temperature

✉ Paweł Stoch
    pstoch@agh.edu.pl

1   Faculty of Materials Science and Ceramics, AGH University
     of Science and Technology, ul. Mickiewicza 30,
     30-059 Kraków, Poland

2   Institute of Electron Technology Kraków Division, ul.
     Zabłocie 39, 30-701 Kraków, Poland

up to about 140 °C, and then rapid desorption is observed [27]. On the other hand, P_2O_5 is the main building oxide of phosphate glasses network. Water corrosion of the glass network leads to its partial depolymerization.

The glass network connectivity can be described using O/P ratio. The vitreous P_2O_5 creates a three-dimensional phosphate network with O/P = 2.5. The increase in the ratio results in the gradual depolymerization of the phosphate network. The full depolymerization is achieved for orthophosphate stoichiometry with O/P ratio over 4 [30].

Addition of Al_2O_3 decreases the number of P–O–P linkages by replacing them by P–O–Al which are much more hydration resistant. Thus, chemical durability of the glasses is increased and it is one of the highest achieved durabilities for the glass of composition $60P_2O_5$–$40Al_2O_3$ [21]. This glass is characterized by the formal O/P ratio equaling 3.5 and belongs to polyphosphate glasses. Phosphate network in this glass is composed of very short phosphate chains created mainly by P_2O_7 dimmers which are joined by Al^{3+} oxygen polyhedrons. The Al polyhedrons increase the glass network connectivity and, thus, increase polymerization of the whole network. Aluminum ions are intermediate compounds and can be glass network formers or modifiers depending on their coordination number to oxygen. They can be glass network formers in coordination 4 and modifiers in coordination 6. In the case of iron–phosphate glasses, it was found out that the glass leachability is independent of the role of iron in the glass network [31]. A similar behavior is also valid for aluminum–phosphate glasses [29].

The subject of the studies is aluminum–phosphate glasses of composition $60P_2O_5$–$(40-x)Al_2O_3$–xNa_2O. The glasses are characterized by constant P_2O_5 concentration, whereas Al_2O_3 is gradually substituted by Na_2O in the range from 5 to 30 mol%. The formal O/P ratio is in the range from 3.42 to 3 for x = 5 and 30, respectively. Thus, all of them belong to the polyphosphate glass region where the phosphate network is built of chains. The length of the chains increases with Na_2O content. Then, the glass network for x = 5 is composed of very short chains (dimmers) which are connected by Al oxygen polyhedrons, in which the number of P–O–P bonds is strongly limited. On the other side, in the case of the x = 30 glass, the phosphate chains are much longer and their connectivity via Al oxygen polyhedrons is considerably lower and the number of P–O–P bonds is higher.

From the waste vitrification point of view, an increase in Al_2O_3 should improve considerably the chemical durability, which is a strongly desired effect. On the other hand, Al_2O_3 by an increase in the glass network connectivity may increase the network rigidity and vitrification temperature [26, 32], which may limit their potential application in waste immobilization.

Taking all into account, the aim of the studies was to describe thermal properties and leachability of $60P_2O_5$–$(40-x)Al_2O_3$–xNa_2O glasses from the waste immobilization point of view.

Experimental methods

Phosphate glasses of the composition $60P_2O_5$–$(40-x)Al_2O_3$–xNa_2O in mol% were prepared from chemically pure $NH_4H_2PO_4$, Al_2O_3, and Na_2CO_3. Approximately 20 mass% overweight of $NH_4H_2PO_4$ was used to compensate P_2O_5 losses during melting of the batch due to evaporation. Batches were melted for 2 h at 1300 °C in Al_2O_3 crucible in an electric furnace with the furnace atmosphere as close to natural as possible. The chemical composition of the obtained glasses was checked by X-ray fluorescence (XRF) and was similar to the assumed in the uncertainty of the method. All samples were XRD-checked to be amorphous. The chemical composition and the samples designation are shown in Table 1.

Heating microscopy thermal analysis was carried out using compacted powder samples of a cubic shape. Powdered samples were prepared by milling of bulk samples in a ball mill. Then, they were wetted in ethanol and compacted to cubes of $3 \times 3 \times 3$ mm by a hand press. The observations of the shape changes during heating were conducted in a Carl Zeiss MH01 microscope at a heating rate 10 °C min^{-1}. Data of the sample height were collected at intervals of 10 °C during the experiment, and shrinkage curves were obtained. The beginning of the sintering process temperature T_s as the onset of densification was determined from the shrinkage curve. The half-sphere temperature T_{hs}, which was the temperature at which the height of the sample was half the width of the base, and the flow temperature T_f, which was the first temperature at which the sample is melted to a third of its original height, were observed [26]. Additionally, shrinkage (h/h_0—ratio of a sample height at give temperature to the height at room temperature) dependence on temperature was determined.

Glass transformation temperature T_g at the half of the heat capacity step on DSC curve, crystallization T_C as the onset of the first crystallization peak and melting T_M as the

Table 1 Chemical composition of the glasses/mol%

Oxide	PAN1	PAN2	PAN3	PAN4	PAN5	PAN6
P_2O_5	60	60	60	60	60	60
Al_2O_3	35	30	25	20	15	10
Na_2O	5	10	15	20	25	30

first melting peak maximum temperature were measured by differential scanning calorimetry (DSC) method combined with thermogravimetry (TG) at the heating rate 10 °C min^{-1}. Measurements were carried out using Netzsch STA 449 F5 Jupiter, operating in the heat flux DSC mode. Glass powder samples weighing 80 mg were heated in Al$_2$O$_3$ crucibles at a rate of 10 C min^{-1} in a dry air atmosphere up to 1100 °C. Characteristic temperatures of the glass transformation effects and changes in specific heat at T_g were determined applying the Netzsch Proteus Thermal Analysis Program (version 5.0.0.).

Water leachability studies were conducted according to the ASTM C1285-02 test (PCT—product consistency test) which now is one of the mostly conducted protocols, thus giving an easy way to compare different glasses with each other, especially those which are used in waste immobilization. The glass samples were crushed, and standard sieve analysis was performed with top sieve of screen openings of 0.15 mm and the lower with the openings of 0.075 mm. The sieves were placed in a mechanical shaker. The shaking time was 30 min. Thus, the glass of a grain size in the range of 0.075–0.150 mm was obtained. 1.5 g of grains was put into PTFE bottles, and 15 mL of de-ionized water was added. The bottles were sealed and placed in a laboratory oven at 90 °C for 7 days. Then, the solution was filtered off. The chemical composition of the solution was analyzed using inductively coupled plasma atomic emission spectroscopy (ICP-AES) method. The results of leaching tests were presented as normalized leaching coefficient of element i (NL$_i$) according to the formulae $NL_i = (C_i V_i)/(f_i S_A)$, where C_i is the concentration of the element i in the solution, V_i is the solution volume, f_i is the mass percentage of the i element in the glass, and S_A is the surface of the tested sample, as recommended by the standard.

Results and discussion

Heating microscopy

Observation of the glasses shape change during heating was conducted in the heating microscope. Depending on the samples composition, three different behaviors of the change were evidenced: the first one for the glasses of low Na$_2$O content as PAN1 and PAN2, the second range for the samples PAN3, PAN4, and PAN5 and the last for PAN6. For all the glasses, temperature dependence of the shrinkage was determined. The exemplary curves for the above three regions are presented in Fig. 1, and the determined characteristic temperatures for all the glasses are summarized in Table 2.

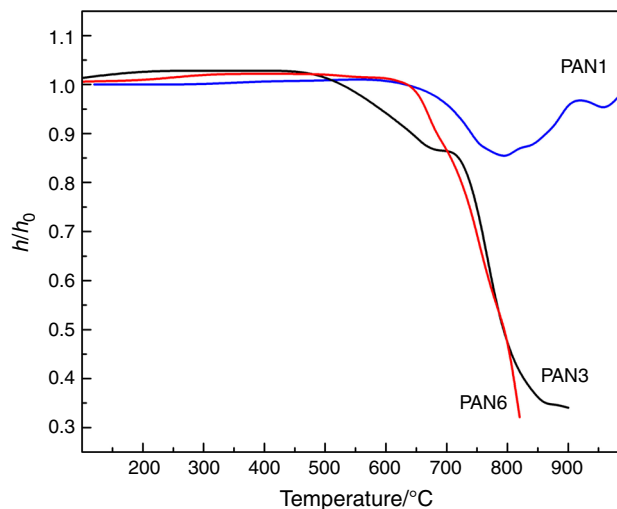In the case of the low Na$_2$O content glasses (PAN1 and PAN2), their temperature behavior in the heating

Fig. 1 Dependence of the glass shrinkage on temperature

Table 2 Characteristic temperatures of the studied glasses

Glass	T_S/°C	T_{hs}/°C	T_f/°C
PAN1	620 (10)		
PAN2	550 (10)		
PAN3	527 (10)	790 (10)	900 (1)
PAN4	520 (10)	780 (10)	810 (10)
PAN5	425 (10)	730 (10)	750 (10)
PAN6	630 (10)	790 (10)	820 (10)

microscopy is similar. Sintering is observed as densification of the samples with maintaining the shape of the sample. After densification which is achieved in the shrinkage curve minimum, the samples start to change the shape and some rounding of the edges is observed. Rounding of the edges suggests an appearance of a liquid phase. This takes place at around 800 °C in both cases. Then, the samples start to expand and the effect is stopped at about 1000 °C. For the higher temperatures, the shape becomes constant up to 1450 °C. Such a behavior may be due to crystallization of the glasses at temperatures around 800 °C when crystal phases of high-temperature melting points are formed. In the case of high-alumina-content glasses such as PAN1 and PAN2, crystallization of AlPO$_4$ and Al(PO$_3$)$_3$ can be expected [23] which both have a melting point above the maximum temperature limit of the equipment.

The higher Na$_2$O content samples for x from 15 to 25 (PAN2–PAN5) show shape change typical for glasses. Densification with about 20% shrinkage is observed, and the sintering temperature decreases with the Na$_2$O increase. After sintering, a characteristic plateau is observed, in which the sample shape is constant. Then is evidenced

rounding of the samples corners, which is related to the formation of a liquid phase and the fast shrinkage begins with the formation of round shape which became a half-sphere until flow point is achieved.

The highest Na_2O content glass (PAN6) shows behavior which is rather typical for crystalline phase melting. The height of the sample is unchanged up to over 630 °C when strong shrinkage is evidenced. Although over about 450 °C a formation of a small quantity of a liquid phase which smoothed the surface is observed, the shape and the height are maintained. The rapid melting without a formation of a characteristic for glasses' spherical shape is registered. This means the low viscosity of the melt is specific for crystalline samples melting.

Taking into account waste immobilization technology, all the samples are characterized by a low sintering temperature with the formation of the liquid phase. In the case of the low Na_2O content glasses, the crystallization effect with the formation of the high melting phases limits their practical application in the case of waste vitrification. On the other hand, taking into consideration only sintering temperatures, the glasses can be used to prepare glass–composite materials, which are a new possibility in waste immobilization [20, 21]. The obtained characteristic temperatures for the glasses from the mid-Na_2O content region may indicate the usefulness of the glasses in the waste vitrification technique.

DSC studies

DSC curves for all the studied glasses are shown in Fig. 2. Transformation (T_g), crystallization (T_c), liquidus (T_l) temperatures, change in the specific heat capacity
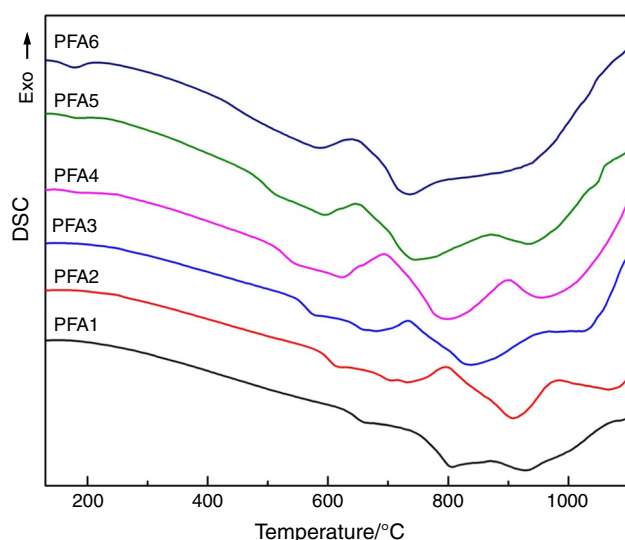
accompanying the glass transformation (ΔC_p), and Hruby's glass thermal stability (K_H) criterion are summarized in Table 3.

All the samples show the characteristic for glasses, a transformation step in which temperature decreases with increasing Na_2O content. Behind the step appears an exothermic effect of crystallization, which becomes stronger when sodium is added. The crystallization peak is broad, suggesting a complex process of crystallization. After the peak, an endothermic effect is observed which can be related to melting or partial melting of the crystalline phases. It is worthy to mention that close inspection of the curves showed that for the glasses over $x = 20$ (PAN4) a small endothermic effect at about 180 °C is evidenced. The effect is stronger with the increase in sodium in the glass and may be related to rapid water desorption [27].

Comparing the obtained glass transition temperatures with the sintering temperatures, we observed that the T_g temperatures lie higher than those of the sintering in all cases, except the last glass sample. On the other hand, the presented glass transition temperatures were obtained as usual in the midpoint of the transition, whereas the sintering temperature is usually determined as the onset of densification. Comparing the glass transition onset temperature with the obtained sintering point, we found a good agreement between these temperatures in the uncertainty limit of the methods. In the case of the PAN6 sample, the sintering temperature is considerably higher. On the other hand, the small quantity of a liquid phase was observed at 450 °C, which is close to the determined T_g value. Thus, one can see that the sintering of the powdered samples takes place in the glass transition temperature. The decrease in the T_g temperature with the increase in Na_2O may be related to the increase in the glass network flexibility due to the increasing length of the phosphate chains.

The evaluated T_L temperatures as the endothermic effect next to the crystallization peak on the DSC curves lie

Fig. 2 DSC curves of the studied glasses

Table 3 Transformation (T_g), crystallization (T_c), liquidus (T_l) temperatures, change in the specific heat capacity accompanying the glass transformation (ΔC_p), and Hruby's glass thermal stability (K_H) for the studied glasses

Glass	T_g/°C	T_c/°C	T_L/°C	ΔC_p/Jg^{-1}K^{-1}	K_H
PAN1	647 (1)	814 (1)	929 (1)	0.187	0.688
PAN2	603 (1)	731 (1)	909 (1)	0.296	1.391
PAN3	564 (1)	676 (1)	838 (1)	0.297	1.446
PAN4	529 (1)	632 (1)	797 (1)	0.244	1.602
PAN5	492 (1)	595 (1)	744 (1)	0.241	1.447
PAN6	435 (1)	592 (1)	739 (1)	0.069	0.936

between T_{hs} and T_f temperatures for the samples over 15 mol% of Na$_2$O, which is in accordance with the heating microscopy observation. In the case of the lower Na$_2$O content samples in heating microscope, we do not observe typical melting. On the other hand in the T_L region, formation of the residual liquid phase is evidenced. This may be due to the melting of the sodium-containing crystal phases, and the main aluminum phosphate phases are preserved.

TG analysis

TG analysis of the high-sodium-content samples revealed the existence of two small mass-loss regions. Exemplary TG curve is presented in Fig. 3. The first region at low temperatures was designated as Δm_1 and the second one at high temperatures as Δm_2. The determined mass losses in these regions are summarized in Table 4.

In the case of the sample PAN1, we do not observe any mass losses in the measured temperature range. When the Na$_2$O content is increased, the high-temperature mass loss is evidenced. The beginning of the mass change is for all the samples at the same temperature over about 1000 °C. We were not able to observe the end of the change, and therefore, in the table Δm_2 values are for the temperature range from 1000 to 1100 °C. A slight increase in the Δm_2 is also observed with an increase in Na$_2$O content in the glass. The increase in Na$_2$O results in an increase in the liquid phase quantity at high temperatures. Thus, the mass loss is probably related to the evaporation of P$_2$O$_5$ from the melted glass. For the highest sodium content glasses, the low temperature mass-loss region is also evidenced, which begins at the same temperature about 180 °C for all the samples. The mass change increases with Na$_2$O content in the glass. This may be related to the release of H$_2$O bonded
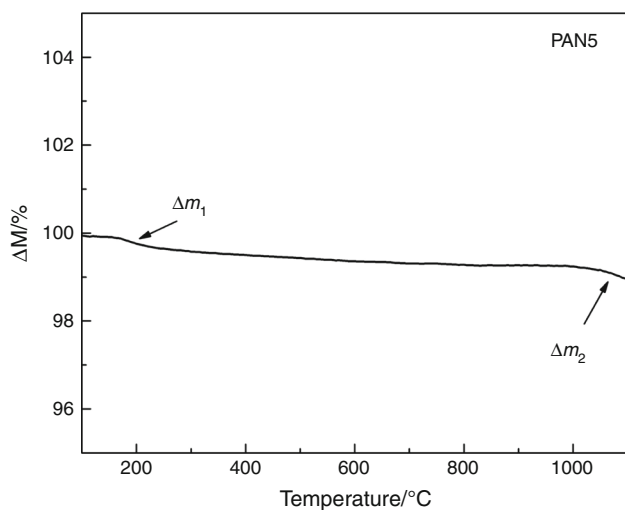
Table 4 Mass losses in low (Δm_1) and high (Δm_2) regions

Glass	Δm_1/%	Δm_2/%
PAN1		
PAN2		− 0.25(2)
PAN3		− 0.26(2)
PAN4	− 0.11(1)	− 0.30(2)
PAN5	− 0.23(1)	− 0.32(2)
PAN6	− 0.53(1)	− 0.33(2)

Table 5 Normalized elemental release rates of the glass elements (NL_i) after 7 days

Glass	NL_P/g m^{-2}	NL_{Al}/g m^{-2}	NL_{Na}/g m^{-2}
PAN 1	0.108	0.004	0.333
PAN 2	0.973	0.013	0.415
PAN 3	3.884	0.057	1.111
PAN 4	29.180	0.549	6.654
PAN 5	43.882	2.167	6.445
PAN 6	164.187	22.826	20.695

in the glass network, which is supported by the observation of the small endothermic effect at the same temperature on the corresponding DSC curves. By this fact, the usability of PAN4 to PAN6 glasses in waste immobilization is strongly limited. Additionally, the evidenced mass loss over 1000 °C makes the high-temperature limit of the glasses' usability in waste vitrification process.

Water leachability results

The obtained normalized elemental release rates for the investigated glasses are summarized in Table 5.

According to ASTM C1288-02 test, the values of NL_i should be below certain limits so that the glass could be considered suitable for waste immobilization. The standard was created for borosilicate glasses, but in both cases, sodium is the most leached element. The NL_{Na} for sodium needs to be below 5.05 g m^{-2} after 7 days to fulfill the standard limit. The glasses' water resistance decreases considerably with the Na$_2$O increase. Only the first three glasses of the lowest sodium content to 15 mol% of Na$_2$O fulfill the standard limit. Their water resistance is superior although the leachability results for the tested glasses are comparable or even better than for other phosphate glasses considered as a matrix for waste vitrification [23, 29].

Conclusions

All of the investigated glasses were synthesized in a conventional way by casting the melt on a steel plate. During the synthesis, over about 1000 °C, strong evaporation of

Fig. 3 TG curve of the PAN5 glass

P_2O_5 is expected, and therefore, some overweight of the oxide should be used to compensate the mass loss.

The glasses of the lowest Na_2O content (5 and 10 mol%) during heating go under crystallization effect with the formation of the high-temperature-melting aluminum phosphates. On the other hand, the glasses are characterized by superior water durability. The first effect confines their usability in waste vitrification. Nevertheless, the glasses can be valuable in waste immobilization by sintering the waste with glass frit and production of glass–ceramic materials. The sintering temperature is rather low, and leachability results are very good.

The glass containing 15 mol% of Na_2O seems to be the most optimal for waste vitrification process. Due to low melting temperature, the short plateau on the shrinkage curve indicates rather low viscosity what should proceeds in a shortening of vitrification time and lowering the melting temperature comparing to borosilicate. Thus, the vitrification total costs should be reduced. The glass is also characterized be very good water durability, which may ensure the safe storage of the vitrified final product.

The glasses of the higher Na_2O content over 20 mol% also have good thermal properties, but their application, in this case, is limited due to their water corrosion.

References

1. Wilder JA. Glasses and glass ceramics for sealing to aluminum alloys. J Non Cryst Solids. 1980;38–39:879–84.
2. Sales BC. Phosphate glasses. MRS Bull. 1987;12:32–5.
3. Hench LL. Bioceramics: from concept to clinic. Am CeramSoc Bull. 1993;72:93–8.
4. Ogino M, Hench LL. Formation of calcium phosphate films on silicate glasses. J Non Cryst Solids. 1980;38–39:673–8.
5. Fletcher JP, Kirkpatrick RJ, Howell D, Risbud SH. ^{31}P Magic-angle spinning nuclear magnetic resonance spectroscopy of calcium phosphate glasses. Faraday Trans. 1993;89:3297–9. https://doi.org/10.1039/FT9938903297.
6. Knowles JC. Phosphate based glasses for biomedical applications. J Mater Chem. 2003;13:2395–401. https://doi.org/10.1039/B307119G.
7. Abou Neel EA, Pickup DM, Valappil SP, Newport RJ, Knowles JC. Bioactive functional materials: a perspective on phosphate-based glasses. J Mater Chem. 2009;19:690–701. https://doi.org/10.1039/B810675D.
8. Broer MM, Bruce AJ, Grodkiewicz WH. Photoinduced refractive-index changes in several Eu^{3+}, Pr^{3+}, and Er^{3+}-doped oxide glasses. Phys Rev B. 1992;45:7077–83. https://doi.org/10.1103/PhysRevB.45.7077.
9. Carini G, D'Angelo G, Tripodo G, Fontana A, Rossi F, Saunders GA. Low-energy magnetic excitations in the Pr metaphosphate glass. EPL Europhys Lett. 1997;40:435.
10. Durville FM, Behrens EG, Powell RC. Laser-induced refractive-index gratings in Eu-doped glasses. Phys Rev B. 1986;34:4213–20. https://doi.org/10.1103/PhysRevB.34.4213.
11. Dong-Bing H, Chun-Lei Y, Ji-Meng C, Shun-Guang L, Li-Li H. A novel Ce^{3+}/Tb^{3+} codoped phosphate glass as down-shifting materials for enhancing efficiency of solar cells. Chin Phys Lett. 2010;27:114208.
12. Liang X, Zhu C, Yang Y, Yuan S, Chen G. Luminescent properties of Dy^{3+}-doped and Dy^{3+}–Tm^{3+}co-doped phosphate glasses. J Lumin. 2008;128:1162–4.
13. Saunders GA, Brennan T, Acet M, Cankurtaran M, Senin HB, Sidek HAA, et al. Elastic and non-linear acoustic properties and thermal expansion of cerium metaphosphate glasses. J Non Cryst Solids. 2001;282:291–305.
14. Cramer AJ, Cole JM, FitzGerald V, Honkimaki V, Roberts MA, Brennan T, et al. Effects of rare-earth co-doping on the local structure of rare-earth phosphate glasses using high and low energy X-ray diffraction. Phys Chem Chem Phys. 2013;15:8529–43. https://doi.org/10.1039/C3CP44298E.
15. Wacławska I, Szumera M, Stoch P, Sitarz M. Structural role of Fe in the soil active glasses. Spectrochim Acta—Part A Mol Biomol Spectrosc. 2011;79:728–32.
16. Szumera M, Waclawska I, Olejniczak Z. Influence of B_2O_3 on the structure and crystallization of soil active glasses. J Therm Anal Calorim. 2010;99:879–86. https://doi.org/10.1007/s10973-009-0550-1.
17. Kuczek J, Jeleń P, Stoch P, Błachowski A, Wacławska I, Szumera M. Raman and Mössbauer studies of iron phosphate-silicate glasses. J Mol Struct. 2018;1170:82–9.
18. Musinu A, Piccaluga G, Pinna G. Structural properties of lead-iron phosphate glasses by X-ray diffraction. J Non Cryst Solids. 1990;122:52–8.
19. Selvaraj U, Rao KJ. Transport properties of phosphomolybdate and phosphotungstate glasses. Philos Mag Part B. 1988;58:203–16. https://doi.org/10.1080/13642818808208481.
20. Ojovan MI, Lee WE. An introduction to nuclear waste immobilisation. Amsterdam: Elsevier Science; 2014.
21. Donald IW. Waste immobilization in glass and ceramic based hosts: radioactive, toxic and hazardous wastes. Hoboken: Wiley; 2010.
22. Bingham PA, Hand RJ, Scales CR. Immobilization of simulated plutonium-contaminated material in phosphate glass: an initial scoping study. In: Materials research society symposia proceedings of scientific basis for nuclear waste management XXIX, Ghent, Belgium. vol 932. 2006. p. 345–52.
23. Stoch P, Ciecinska M. Thermochemistry of phosphate glasses for immobilization of dangerous waste. J Therm Anal Calorim. 2012;108:705–9.
24. Stoch P, Ciecinska M, Stoch A. Thermal properties of phosphate glasses for salt waste immobilization. J Therm Anal Calorim. 2014;117:197–204.
25. Kim C-W, Day DE. Immobilization of Hanford LAW in iron phosphate glasses. J Non Cryst Solids. 2003;331:20–31.
26. Ciecińska M, Stoch P, Stoch A, Nocuń M. Thermal properties of $60P_2O_5$–$20Fe_2O_3$–$20Al_2O_3$ glass for salt waste immobilization. J Therm Anal Calorim. 2015;121:1225–32. https://doi.org/10.1007/s10973-015-4586-0.

27. Palavit G. Phospahte glasses and water. Phosphorus Res. Bull. 1996;6:85–90.
28. Bunker BC, Arnold GW, Wilder JA. Phosphate glass dissolution in aqueous solutions. J Non Cryst Solids. 1984;64:291–316.
29. Ma L, Brow RK, Schlesinger ME. Dissolution behavior of Na$_2$O–FeO–Fe$_2$O$_3$–P$_2$O$_5$ glasses. J Non Cryst Solids. 2017;463:90–101.
30. Brow RK. Review: the structure of simple phosphate glasses. J Non Cryst Solids. 2000;263:1–28.
31. Karabulut M, Marasinghe GK, Ray CS, Day DE, Waddill GD, Booth CH, et al. An investigation of the local iron environment in iron phosphate glasses having different Fe(II) concentrations. J Non Cryst Solids. 2002;306:182–92.
32. Brow RK. Nature of alumina in phosphate glass: I, properties of sodium aluminophosphate glass. J Am Ceram Soc. 1993;76:913–8. https://doi.org/10.1111/j.1151-2916.1993.tb05315.x.